Exp.-Nr.: A1/01–12
Eingang:
an PAC:

Mainz Microtron MAMI

Collaboration: A1

Spokesperson: H. Merkel

Title: Measurement of the elastic $A(Q^2)$ form factor of the deuteron at very low momentum transfer and the extraction of the monopole charge radius of the deuteron

Authors: P. Achenbach[1], R. Böhm[1], D. Bosnar[2], J. Beričič[3], L. Debenjak[3], A. Denig[1], M. O. Distler[1], A. Esser[1], H. Fonvieille[4], I. Friščić[2], M. Gómez Rodríguez[1], K. Griffioen[5], S. Kegel[1], Y. Kohl[1], H. Merkel[1], M. Mihavilovič[1], U. Müller[1], J. Pochodzalla[1], T. R. Saito[1], B. S. Schlimme[1], M. Schoth[1], F. Schulz[1], C. Sfienti[1], I. Sick[6], S. Širca[3], M. Thiel[1], A. Weber[1]

[1] Institut für Kernphysik, Johannes Gutenberg-Universität, Mainz

[2] Department of Physics, University of Zagreb, Croatia

[3] University of Ljubljana and Institute "Jožef Stefan", Ljubljana, Slovenia

[4] IN2P3-CNRS, Université Blaise Pascal, Clermont-Ferrand, France

[5] Department of Physics, College of William and Mary, Williamsburg, VA

[6] Departement für Physik, Universität Basel, Switzerland

Contactpersons: M. O. Distler, K. Griffioen

Abstract of physics: We propose to perform a high precision measurement of the elastic cross section in the reaction ^{2}H(e,e')d at very low 4-momentum transfer squared, Q^2. The data will be used to extract the elastic $A(Q^2)$ and $G_C(Q^2)$ form factors of the deuteron and the monopole charge radius. The contributions of the magnetic and the quadrupole form factor in the low Q^2 region are small and known to a good precision from previous measurements. There is renewed interest in the charge radius of the deuteron as it may help to solve the proton radius puzzle in combination with new Lamb shift measurements at PSI.

Abstract of equipment: Standard A1 equipment with the liquid deuterium target.

MAMI specifications :

beam energy:	min. 180 MeV	max. 450 MeV
beam current:	min. 25 nA	max. 15 μA
time structure:	continuous beam	
polarization:	no	

Experiment specifications:

targets and chamber:	liquid deuterium target, 5cm cell
hall:	spectrometer hall
beam line:	standard to spectrometer hall

spectrometer:	particles:	range of angles:	out of plane:
SpekA	e,p	$18^\circ - 160^\circ$	—
SpekB	e,p	$7^\circ - 62^\circ$	—
SpekC	e	$18^\circ - 160^\circ$	—

Beam time request :

set-up without beam:	4 days
set-up with beam:	90 h
data taking:	160 h

1 Introduction and Motivation

Ever since Hofstadter first fired a high-energy electron at an atomic nucleus [1], electron scattering has been the preferred technique for accurately measuring nuclear charge distributions. In its simplest conception, a mono-energetic electron beam acts like a plane wave that scatters coherently from all the points of charge in an extended object. The resulting Fraunhofer diffraction pattern is the Fourier transform of the charge density. Specifically, for elastic scattering from a proton, the cross section is

$$\frac{d\sigma}{d\Omega} = \left(\frac{d\sigma}{d\Omega}\right)_{\text{Mott}} \frac{1}{\epsilon(1+\tau)} \left[\tau G_M^2(Q^2) + \epsilon G_E^2(Q^2)\right] \tag{1}$$

Here, E is the electron beam energy, E' is the scattered electron energy, $\nu = E - E'$ is the energy transfer, θ is the electron's scattering angle in the lab frame where the proton is at rest, M is the mass of the target proton, $Q^2 = 4EE'\sin^2\frac{\theta}{2}$ is the negative squared 4-momentum transfer,

$$\epsilon = \left[1 + 2(1+\tau)\tan^2\frac{\theta}{2}\right]^{-1}, \tag{2}$$

$$\tau = \frac{\nu^2}{Q^2} = \frac{Q^2}{4M^2}, \tag{3}$$

$$\left(\frac{d\sigma}{d\Omega}\right)_{\text{Mott}} = \frac{\alpha^2}{4E^2\sin^4\frac{\theta}{2}} \frac{E'}{E} \cos^2\frac{\theta}{2} \tag{4}$$

is the Mott cross section with recoil factor E'/E, $G_E(Q^2)$ is the electric Sachs form factor, and $G_M(Q^2)$ is the magnetic Sachs form factor. At low Q^2 the form factors can be expressed as

$$G_{E,M}(Q^2) = 1 - \frac{1}{6}\langle r_{E,M}^2\rangle Q^2 + \frac{1}{120}\langle r_{E,M}^4\rangle Q^4 - \frac{1}{5040}\langle r_{E,M}^6\rangle Q^6 + ... \tag{5}$$

in which the moment $\langle r_{E,M}^2\rangle$ is the squared rms charge or magnetic radius. Hence, measurements of the form factor slopes at low Q^2 yield the rms charge and magnetic radii. That is,

$$\left(\frac{dG_{E,M}}{dQ^2}\right)_{Q^2=0} = -\frac{1}{6}\langle r_{E,M}^2\rangle \equiv -\frac{1}{6}\, r_{E,M}^2. \tag{6}$$

A half-century of measurements from various labs has culminated in the recent measurements in Mainz by Bernauer *et al.*[2] who from their data conclude that

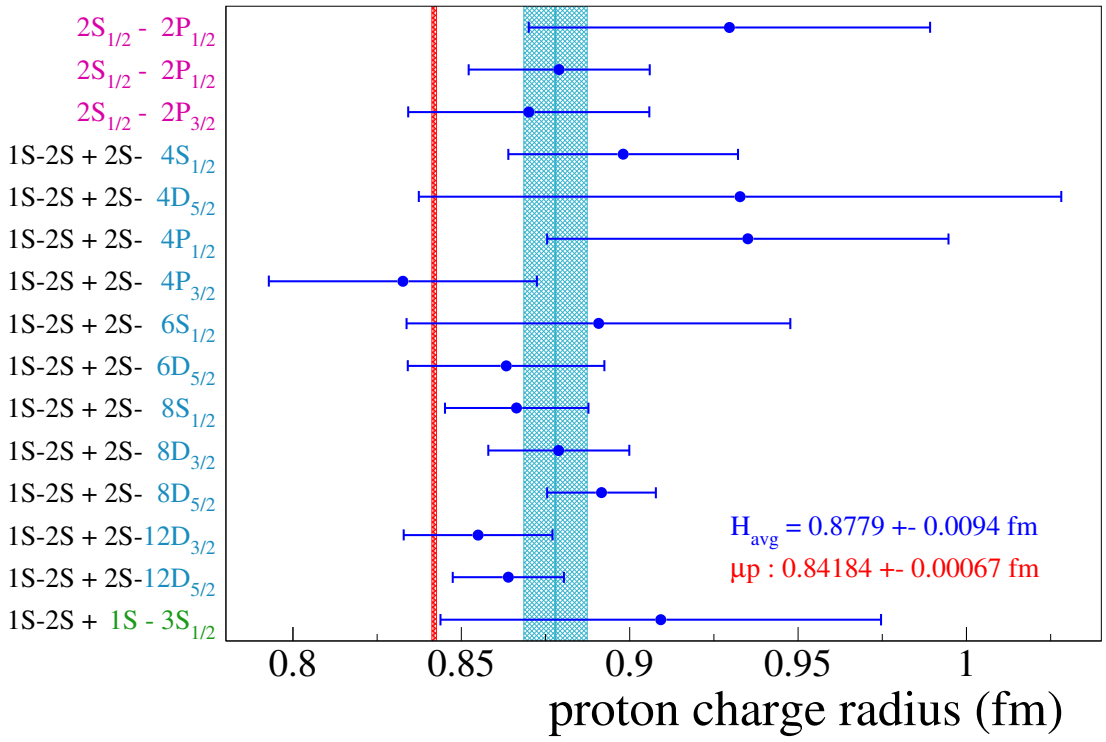

Figure 1: Lamb shift measurements of r_p on hydrogen.

$r_E = 0.879 \pm 0.008$ and $r_M = 0.777 \pm 0.017$ when all errors are added in quadrature.

With the advent of precise atomic experiments using lasers came the ability to measure average properties of nuclear charge distributions from their influence on atomic transitions. Electronic Lamb shift measurements in hydrogen are sensitive to the proton's charge radius r_p (*i.e.* r_E for the proton). Despite the stunning accuracy of the transition frequencies, the small nuclear contributions made uncertainties in the extraction of r_p of similar magnitude to those deduced from electron scattering. Multiple Lamb shift measurements yielded values similar to those extracted from global fits to $G_E(Q^2)$. The hydrogen atom, in effect, had become the world's tiniest electron accelerator, probing the nuclear charge distribution. The CODATA average of electron scattering and Lamb shift results is $r_p = 0.8768(69)$ fm [3].

Several years ago, a new age in precision measurements of the proton size began with the advent of Lamb shift measurements in muonic hydrogen. The muon, being 200 times heavier than the electron, spends its life far closer, on average, to the proton, thereby amplifying the influence of the nuclear charge

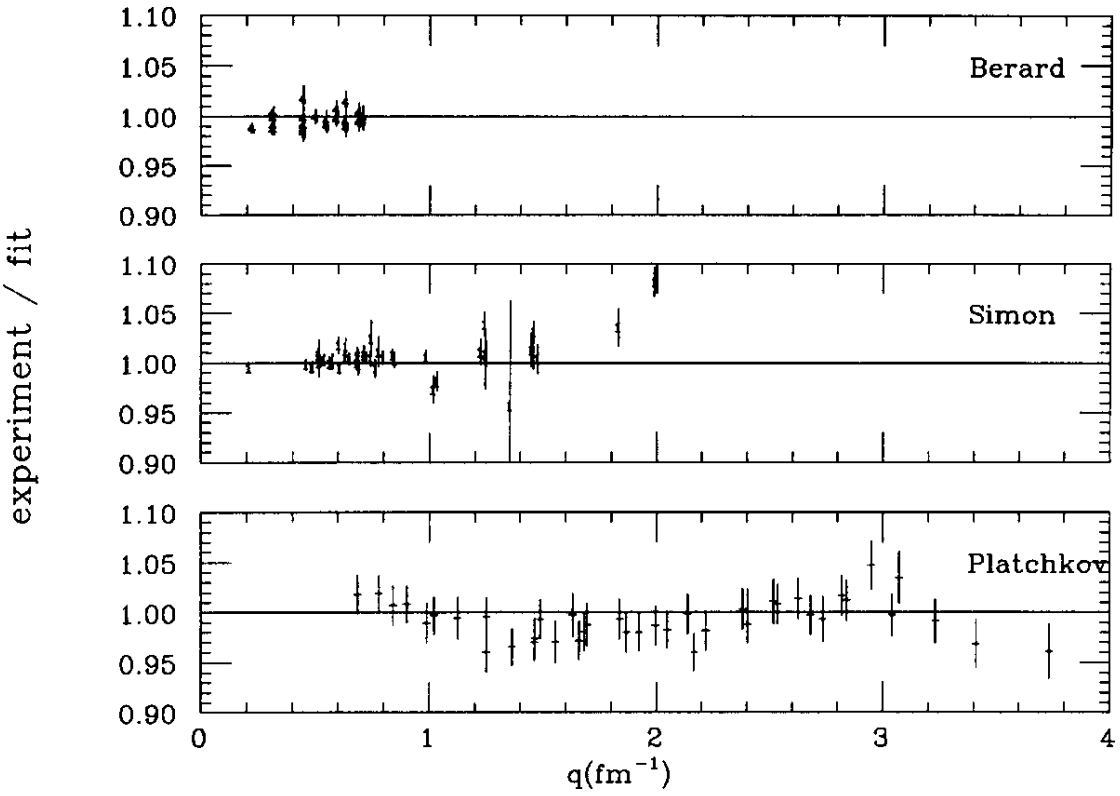

Figure 2: Low-Q^2 electron scattering measurements of r_d on hydrogen [4].

on the atomic levels. The consequent extraction of the proton charge radius is more than an order of magnitude more precise than for the hydrogen Lamb shifts. Pohl *et al.* [5] published a value of $r_p = 0.84184(67)$ from muonic hydrogen, which precipitated the proton size crisis, since this value is several percent below the CODATA value, and differs from it by over 5 standard deviations. In this experiment, the transition energy $\Delta E(2S_{1/2}^{F=1} - 2P_{3/2}^{F=2})$ in μp was measured with 30 ppm precision. In terms of the proton radius, this transition is $\Delta E = 209.9779(49) - 5.2262r_p^2 + 0.0347r_p^3$ meV (milli-electron-volts). The finite-size correction is huge, comprising 2% of the total ΔE. Fig. 1 [6] shows the various hydrogen Lamb shift determinations of r_p in blue, with the blue band indicating the overall best value with error. The red line shows the muonic hydrogen Lamb shift value for r_p.

The proton size puzzle remains unresolved. Prevailing hypotheses include suggestions that individual measurements are somehow inaccurate or that there may be new physics associated with the muon.

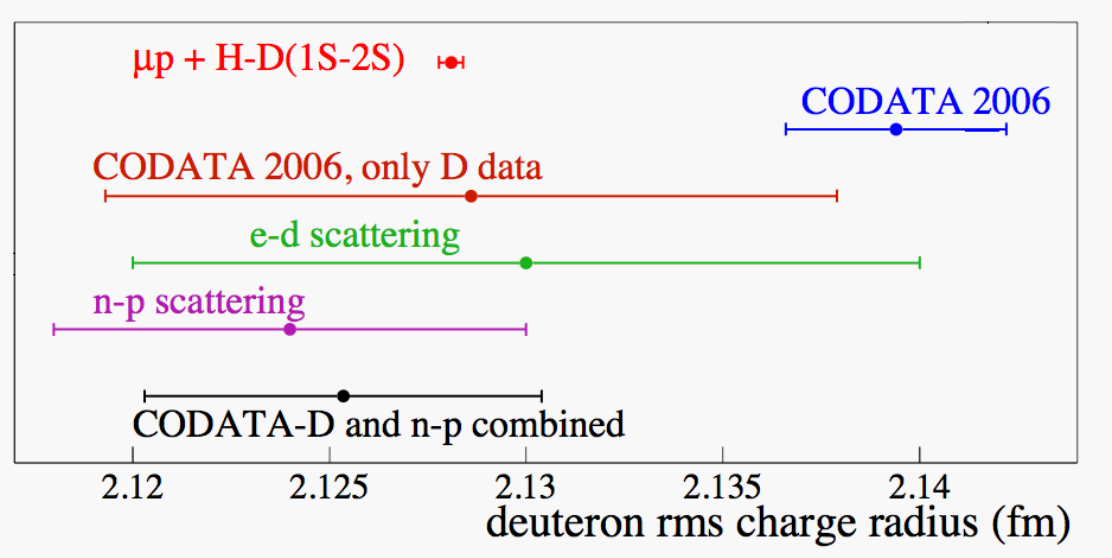

Figure 3: Compilation of world's data on r_d.

1.1 e-d experiment

One of the ways to gain additional insight into the size puzzle is to examine closely another simple system, the deuteron. Sick and Trautmann [4] have done a comprehensive compilation and careful fitting of the deuteron elastic scattering data and have extracted the charge radius $r_d = 2.130 \pm 0.003(\text{stat.}) \pm 0.009(\text{syst.})$. Fig. 2 shows the primary low-Q^2 data from three experiments [7, 8, 9], normalized by the global fit through these points. Meanwhile, the CREMA Collaboration [6] has been measuring the Lamb shift in muonic deuterium. Although there are no results yet forthcoming, the same group has offered an extraction of r_d using isotope-shift data. The isotope shift (2S-1S) between hydrogen and deuterium yields $r_d^2 - r_p^2 = 3.82007(65)$ fm^2. This accuracy is good enough such that when the muonic hydrogen Lamb shift value for r_p is used, $r_d = 2.12808(27)$ fm [6]. This is in agreement with both the CODATA value of $2.1402(28)$ fm and with the best electron scattering value of $2.130(10)$ [4], but with an error that is 50 times smaller! If instead, one were to use the CODATA2006 proton radius, r_d is much larger at $2.1422(28)$. A new, precise deuteron electron scattering measurement can significantly improve on the old measurements and will offer independent input to differentiate between these two deuteron radii, and indirectly shed light on the proton size. Such an experiment is feasible at MAMI with only a few weeks of beam time using the A1 spectrometers configured much like in Bernauer's experiment on the proton. Fig. 3 shows various

determinations of the deuteron radius r_d. The important points to note are the green e-d scattering extraction of Sick [4], the $\mu pH - D(1S - 2S)$ result in red, and the CODATA + H-D(1S-2S) point in blue.
Elastic scattering from the spin-1 deuteron is more complicated than for the proton. The cross section can be written as

$$\frac{d\sigma}{d\Omega} = \left(\frac{d\sigma}{d\Omega}\right)_{\text{Mott}} \left[A(Q^2) + B(Q^2)\tan^2\frac{\theta}{2}\right] \tag{7}$$

in which [4]

$$A(Q^2) = F_{C0}^2(Q^2) + (M_d^2 Q_d)^2 \frac{8}{9}\eta^2 F_{C2}^2(Q^2) + \left(\frac{M_d}{M}\mu_d\right)^2 \frac{2}{3}\eta(1+\eta)F_{M1}^2(Q^2) \tag{8}$$

$$B(Q^2) = \left(\frac{M_d}{M}\mu_d\right)^2 \frac{4}{3}\eta(1+\eta)^2 F_{M1}^2(Q^2)\eta = \frac{Q^2}{4M_d^2}, \tag{9}$$

and

$$F_{C0} \approx 1 - \frac{\langle r_d^2\rangle}{6}Q^2 \tag{10}$$

at low Q^2. In the notation of Abbott [10]

$$\frac{d\sigma}{d\Omega} = \left(\frac{d\sigma}{d\Omega}\right)_{\text{Mott}} \left[G_C^2(Q^2) + \frac{8}{9}\eta^2 G_Q^2(Q^2) + \frac{2}{3}\eta\epsilon^{-1}G_M^2(Q^2)\right] \tag{11}$$

$$\eta = \frac{Q^2}{4M_d^2} \tag{12}$$

$$G_C = F_{C0} \tag{13}$$

$$G_Q = M_d^2 Q_d F_{C2} \tag{14}$$

$$G_M = \left(\frac{M_d}{M}\mu_d\right) F_{M1} \tag{15}$$

$$Q_d = 0.2859\ \text{e fm}^2 \tag{16}$$

$$M_d = 1875.612\ \text{MeV} \tag{17}$$

$$\hbar c = 0.197327\ \text{GeV fm} \tag{18}$$

$$\mu_d = 0.85744\,\mu_N \tag{19}$$

$$M_d^2 Q_d = 25.83 \tag{20}$$

$$\frac{M_d}{M}\mu_d = 1.714 \tag{21}$$

in which G_C is the charge form factor, G_M is the magnetic form factor, G_Q is the quadrupole form factor, Q_d is the deuteron quadrupole moment, and M_d is the deuteron mass. Fig. 4 shows the most recent compilation of the world's deuteron form factor data together with fits by Abbott *et al.* [10].

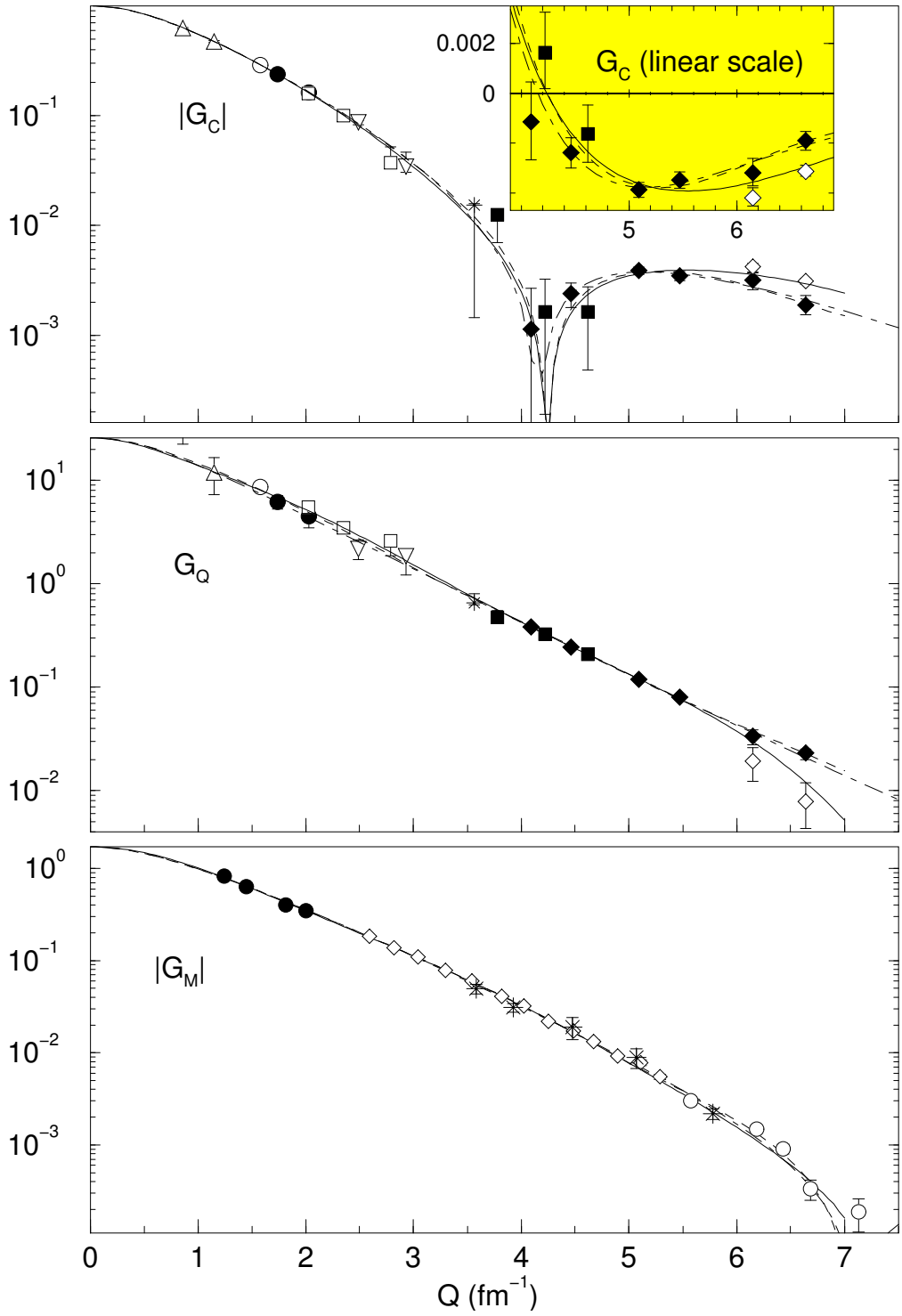

Figure 4: Compilation of world's data plus fits by Abbott *et al.* [10]

One wishes to determine

$$\left(\frac{dG_C}{dQ^2}\right)_{Q^2=0} = -\frac{1}{6} r_d \tag{22}$$

with a statistical accuracy of better than 0.2% with a commensurate systematic error in order to reasonably distinguish between the isotope-shift determinations of r_d using r_p from muonic hydrogen Lamb shifts or r_p from CODATA. Such a measurement will provide important data to help resolve the current puzzle of proton size.

2 Accessible kinematic region and chosen settings

The kinematics setup of an elastic scattering experiment is described completely by any two parameters from the set $\{\epsilon,\, Q^2,\, E,\, E',\, \theta\}$. For the analysis, the most practical combination is Q^2 and ϵ, because the form factors depend only on Q^2 and the relative electric and magnetic contributions to the cross section are weighted by ϵ.

The accessible region is defined through the accelerator and the properties of the detector system. Figure 5 shows the accessible region for an experiment with spectrometer A of the A1-collaboration.

The upper end of the accessible Q^2 region is set by the maximum incident beam energy. MAMI B provides an electron beam with energies up to 855 MeV; the corresponding limit is drawn as a red line in the figure. The maximum beam energy of MAMI C is 1.5 GeV, raising the limit in Q^2 to over 2 GeV^2 (light green area). The lowest Q^2 is set by the lower limit on the incident beam energy (180 MeV, dark green area).

The maximum possible scattering angle determines the lower end of the ϵ region. The maximum backward angle of Spectrometer A is 160°, which excludes the dark blue area. The minimum angle is 22°, setting the higher end of the ϵ region (light blue).

Spectrometer A has a maximum central momentum of 630 MeV/c. This excludes measurements at higher beam energies and forward angles (gray area).

The angular acceptance of Spectrometer A is a little wider than $\pm 4°$, thus a spacing of 2° between the settings gives about 75% overlap to allow checks for systematic errors.

The accelerator can only provide discrete levels of energy with a spacing of 15 MeV (for the existing system), and the change of the energy is quite time-consuming. Therefore, it is best to select a few fixed beam energies. The Mainz proton form factor measurement used constant intervals of 135 MeV, which was

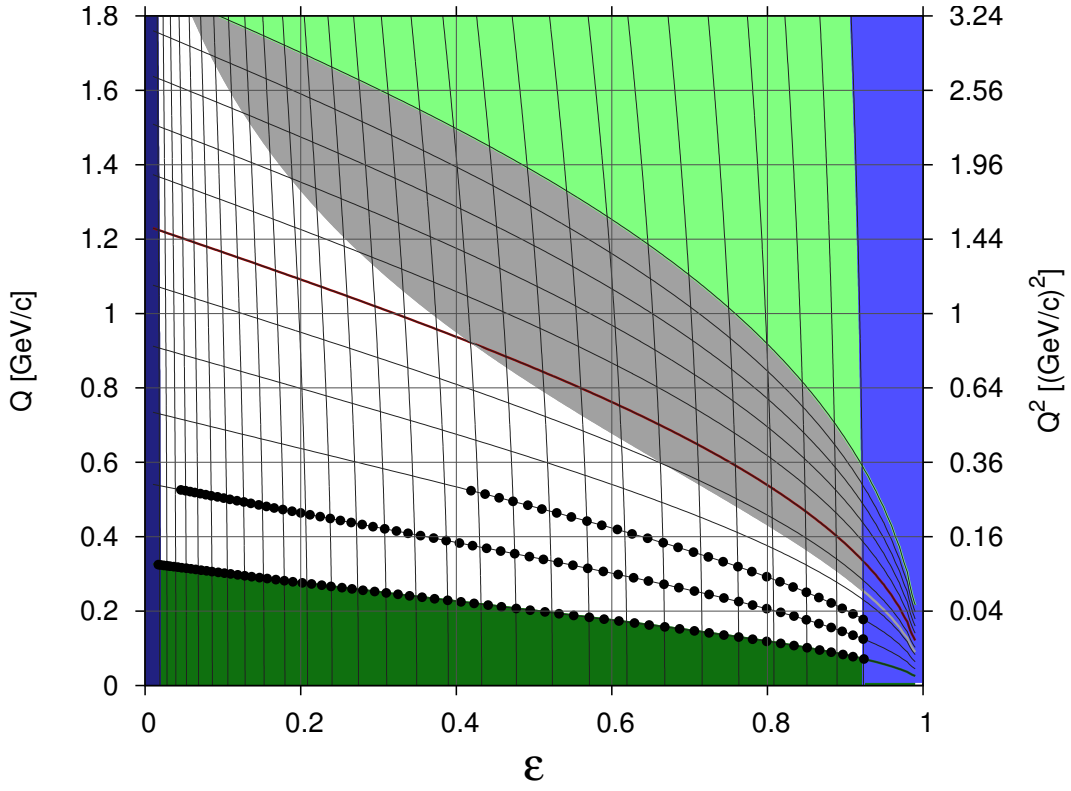

Figure 5: The accessible kinematic region in ϵ/Q-space. The black dots represent the chosen settings (centers of the respective acceptance). The dotted curves correspond to constant incident beam energies in steps of 135 MeV ("horizontal" curves) and to constant scattering angles in 5° steps ("vertical" curves). Also shown are the limits of the facility: The red line represents the MAMI B limit of 855 MeV, with MAMI C it is possible to measure up to the light green curve. The dark (light) blue area shows the kinematic region excluded from measurement due to the maximum (minimum) possible spectrometer angle. The gray shaded region is excluded by the upper momentum of spectrometer A (630 MeV/c).

a trade-off between time and number of setups. However, the proposed experiment here focuses on the extraction of the $A(Q^2)$ form factor at low Q^2, so the lowest possible beam energy of 180 MeV is essential. The measurements at beam energies of 315 and 450 MeV will be used to constrain the normalizations and to check the contributions of the magnetic and quadrupole form factors in the low Q^2 region, which are small and known to a good precision from previous measurements. The maximum sensitivity of the cross section data to the charge radius of the deuteron is expected to be in the region around $1\,\mathrm{fm}^{-1}$ ($Q^2 < 0.04\,\mathrm{GeV}^2$). This region is well-covered be the chosen kinematics.
The resulting setups form a rectangular equidistant grid in E/θ-space, with 135 MeV spacing in E and 2° in θ (black dots in Figure 5).

3 Experimental requirements

The standard setup of the three-spectrometer facility at MAMI will be used [11]. We will control the position of the spectrometer remotely. This system has been successfully installed for the proton form factor measurement [2]. It not only avoids a hall access for every setup change, which would add a large overhead, but it leaves the magnetic elements in the beamline unchanged, which eliminates a source for systematic errors. An unpolarized beam current of 25pA to 15μA will be used. We will use a liquid deuterium target with the standard extended target cell of the A1-collaboration [12]. For some settings, Spectrometer A will be configured to measure the scattered electrons, Spectrometer B will detect the recoil deuterons (see next section). Additionally, for the settings below 62°, the electrons will be measured with Spectrometer B as well, in order to achieve control of systematic uncertainties. Spectrometers A and B sit on opposite sides of the beam line. Therefore, some of the systematic uncertainties introduced by the beam position will cancel out. Spectrometer C will be used to monitor the luminosity.

4 Error control

Due to the construction of Spectrometer A, elastic scattering essentially results in a line on the detector system along which the events are spread out according to the scattering angle, or, equivalently, Q^2. Thus, the local efficiency of the detectors has to be well understood.
As preparatory work for this experiment, the efficiencies of the vertical drift chambers (VDC) have to be studied with high spatial resolution. Recent data from other experiments as well as cosmic ray studies can be used for that pur-

pose. If necessary, the VDC systems of spectrometers A and B have to be uninstalled and opened inside the clean room of the A1 detector laboratory. As described in Ref. [13], broken wires and disrupted electrical connection can be repaired in order to improve the performance of wire chambers. We have not set aside setup time for those tasks as the maintenance of the VDCs does not require exclusive access to the A1 hall. However, a study of the detector efficiencies is part of the beam time estimate.
To this end, for some elastic settings the recoil proton will be measured in coincidence with Spectrometer B (recording all single events in both spectrometers). This "tagging" permits the determination of the local efficiency from the measured single/coincident events ratio. We are confident, that this, together with the redundant measurements with 75% overlap and the techniques developed in Ref. [13], will reduce the influence of these inefficiencies such that they are negligible.
To control the beam properties (luminosity, position), we will use Spectrometer C. It will measure the electrons at rather large backward angles with only a few setup changes over the whole experiment. The number of setups for the luminosity monitor will essentially determine the number of normalization parameters for the final analysis step. In order to achieve the goal of a single normalization parameter per beam energy, high statistic runs are planned to connect different settings for Spectrometer C at times when an angular change for the luminosity monitor cannot be avoided.
A new beam stabilization system has been constructed for the A1 beam line by the B1 collaboration (a comparable system has already been used by the A4 collaboration "parity violating electron scattering"). It has been in operation in the A1 hall for a couple of years now. This will reduce the influence of beam instabilities so that they are negligible.
As part of the setup time without beam we are planning to do a careful geometrical survey of the A1 spectrometer hall. The precise knowledge of the (forward) scattering angles is crucial for this measurement and we will therefore check that beam position, the target position and the rotation axis of the spectrometers match to a precision of better than $1\,\mathrm{mm}$.

5 Method of analysis, error estimates

The beam time for each measurement is determined by the following considerations:

- The maximum current is 15 μA. This will allow a small beam size without the risk of target-boiling.

- The maximum counting rate is 300 Hz. This will limit the dead time. However, the beam-time estimates are based on a rate of 100 Hz in the elastic peak.
- Minimal measuring time per setup is 30 minutes, to get accurate dead time estimates.
- All times are rounded up to the next multiple of 10 minutes.
- The statistical error should be < 0.2% for the whole acceptance.

We estimate the errors in the cross section measurements by the statistical error plus a margin of 0.5% for unaccounted, setup-dependent errors, like deviations in the magnetic field, transfer matrix and angular position of the spectrometer. This leads to an error of less than 1% in every cross section measurement (see Fig. 7). A further increase in beam time for each setting will most likely be futile, since the statistical error would become irrelevant in relation to these other effects.

5.1 Rosenbluth-Separation

The standard way to analyse a form factor measurement is to separate the form factors by a Rosenbluth separation. Exploiting the linear form of Eq. 1, one can separate G_M and G_E at any given Q^2 by measuring several settings at constant Q^2 but different ϵ. This works in a completely model independent way, as long as Eq. 1 holds true. Additionally, to be truly model independent, one has to accept only a very small region around the targeted Q^2 value.
A very similar separation is possible in the case of the spin-1 deuteron (eq. 7). Here, the $A(Q^2)$ and $B(Q^2)$ form factors can be separated by varying the parameter ϵ. The experiment proposed is not designed to separate the form factors. Instead we will rely on previous measurement to subtract the influence of the magnetic and quadrupol form factors. However, we propose to measure at three different beam energies and at backward angles so we should be able to detect any severe deviation from previous measurements of the magnetic form factor.
Fig. 6 shows the deviation of the $A(Q^2)$ form factor and of the square of the charge form factor $G_C(Q^2)^2$ relative to the full calculation including the quadrupole and the magnetic form factor using a parametrization by Abbott *et al.* [10]. The correction at forward angles is small and well understood.

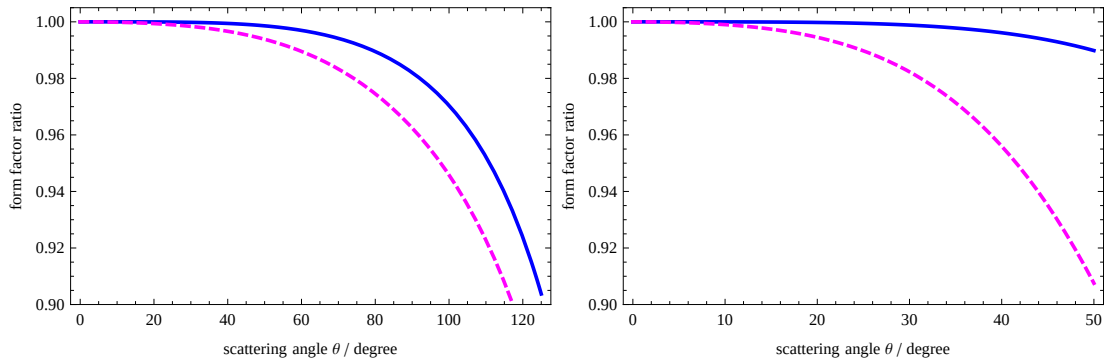

Figure 6: Plot of the $A(Q^2)$ form factor (blue, solid) and the square of the charge form factor $G_C(Q^2)^2$ (magenta, dashed) divided by the normalized cross section $\frac{d\sigma}{d\Omega} / \left(\frac{d\sigma}{d\Omega}\right)_{\text{Mott}}$ as a function of the scattering angle θ for two beam energies 180 MeV (left) and 450 MeV (right). The curves are calculated using a parametrization by Abbott *et al.* [10]

5.2 Global Fit

In the case of the proton form factor the global ansatz for the form factors and the fit directly to the cross sections has proven to be the superior approach compared to the traditional Rosenbluth separation. In order to analyze the deuteron data, we will employ the Sum-of-Gaussian (SOG) parameterization for the form factors. The advantage of the SOG parameterization is that physical constraints like the fall-off of the charge density at large distances can be easily implemented.

6 Beam time request

We request 250 hours of beam-time, according to the following schedule

- 116 setups with durations between 30 and 70 minutes 62h
- 116 setups for empty target runs, 30 minutes each 58h
- 232 setup changes of about 15 minutes 58h
- overhead for overlapping and additional control measurements 40h
- 2 beam energy changes 12h
- calibration runs: 20h

Additionally, we require about 4 days without beam for the survey of the spectrometer angles and the installation of the liquid deuterium target system.

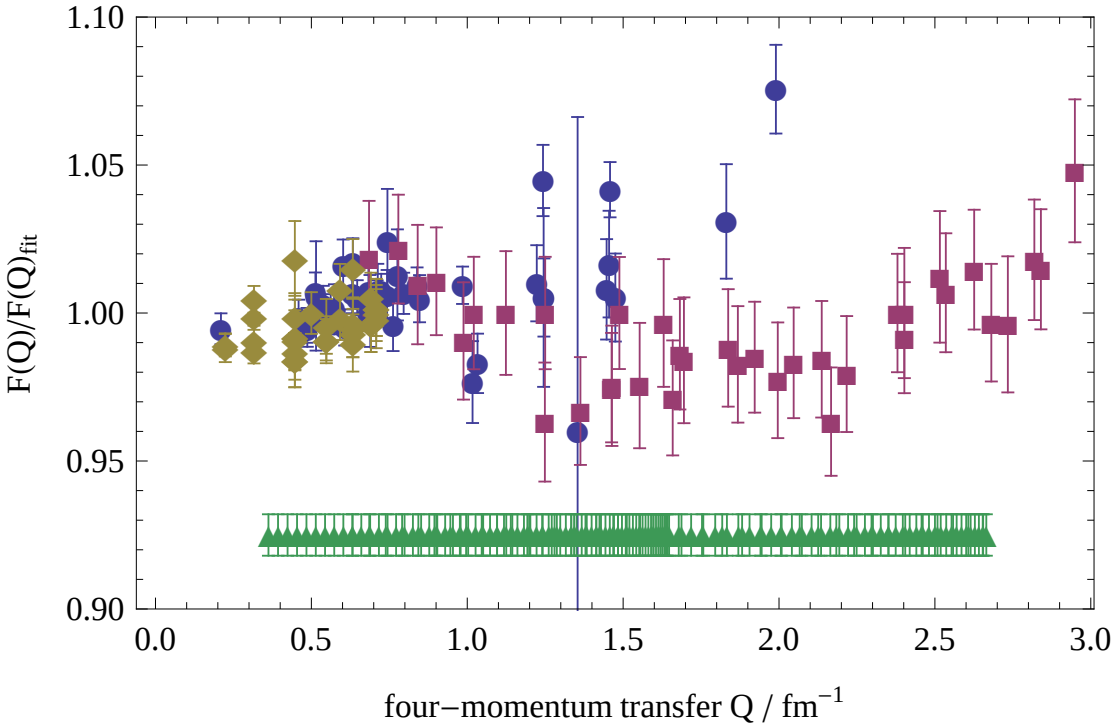

Figure 7: Estimated error for all kinematic settings of the proposed measurement (green triangles). The most precise low-q^2 world data sets (devided by the fit of Abbott et al.) are plotted for comparison: Berard *et al.* [7] (yellow diamonds), Simon *et al.* [8] (blue circles), and Platchkov *et al.* [9] (magenta squares).

7 Possible extensions of the experiment

The proposed experiment focuses on the measurement of the elastic $A(Q^2)$ form factor of the deuteron and the extraction of the charge radius. The analysis relies on the knowledge of the magnetic and the quadrupole form factors, however at low Q^2 their contribution is small and known to a good precision from previous measurements [4, 10].
A direct measurement of the $B(Q^2)$ form factor and the extraction of the magnetic form factor $G_M(Q^2)$ is possible with the Mainz setup. However, it would require measurements at higher beam energies and backward scattering angles.

Those additional kinematics would require several additional weeks of beam time to improve on the precision of previous experiments. A determination of the quadrupole form factor $G_Q(Q^2)$ would require a tensor polarized deuterium target, which is not available at Mainz at the moment.

8 List of planned setups

The following table lists some of the kinematical variables for the proposed settings: beam energy E, scattering angle θ, four-momentum transfer Q, and the polarization parameter ϵ. The last column shows the proposed measuring time in minutes.

E	θ	Q		Q^2	ϵ	time
[MeV]	[°]	[fm^{-1}]	[MeV/c]	[(GeV/c)^2]		[min]
180	23	0.36	72	0.005	0.924	30
180	25	0.39	78	0.006	0.910	30
180	27	0.42	84	0.007	0.897	30
180	29	0.45	90	0.008	0.882	30
180	31	0.48	96	0.009	0.867	30
180	33	0.51	101	0.010	0.851	30
180	35	0.54	107	0.012	0.834	30
180	37	0.57	113	0.013	0.817	30
180	39	0.60	119	0.014	0.799	30
180	41	0.63	125	0.016	0.781	30
180	43	0.66	130	0.017	0.763	30
180	45	0.69	136	0.018	0.744	30
180	47	0.72	141	0.020	0.725	30
180	49	0.74	147	0.022	0.706	30
180	51	0.77	152	0.023	0.687	30
180	53	0.80	158	0.025	0.668	30
180	55	0.83	163	0.027	0.648	30
180	57	0.85	168	0.028	0.629	30
180	59	0.88	173	0.030	0.609	30
180	61	0.90	178	0.032	0.590	30
180	63	0.93	183	0.034	0.571	30
180	65	0.95	188	0.035	0.551	30
180	67	0.98	193	0.037	0.532	30
180	69	1.00	198	0.039	0.514	30
180	71	1.03	203	0.041	0.495	30
180	73	1.05	207	0.043	0.477	30
180	75	1.07	212	0.045	0.458	30
180	77	1.10	216	0.047	0.441	30
180	79	1.12	221	0.049	0.423	30
180	81	1.14	225	0.051	0.406	30
180	83	1.16	229	0.052	0.389	30

E [MeV]	θ [°]	Q [fm^{-1}]	Q [MeV/c]	Q^2 [(GeV/c)^2]	ϵ	time [min]
180	85	1.18	233	0.054	0.372	30
180	87	1.20	237	0.056	0.356	30
180	89	1.22	241	0.058	0.340	30
180	91	1.24	245	0.060	0.325	30
180	93	1.26	249	0.062	0.310	30
180	95	1.28	253	0.064	0.295	30
180	97	1.30	256	0.066	0.280	30
180	99	1.32	260	0.067	0.266	30
180	101	1.33	263	0.069	0.253	30
180	103	1.35	267	0.071	0.239	30
180	105	1.37	270	0.073	0.227	30
180	107	1.38	273	0.075	0.214	30
180	109	1.40	276	0.076	0.202	30
180	111	1.41	279	0.078	0.190	30
180	113	1.43	282	0.080	0.179	30
180	115	1.44	285	0.081	0.168	30
180	117	1.46	288	0.083	0.157	30
180	119	1.47	290	0.084	0.147	30
180	121	1.48	293	0.086	0.137	30
180	123	1.50	295	0.087	0.128	30
180	125	1.51	298	0.089	0.119	30
180	127	1.52	300	0.090	0.110	30
180	129	1.53	302	0.091	0.102	40
180	131	1.54	304	0.093	0.094	40
180	133	1.55	306	0.094	0.086	50
180	135	1.56	308	0.095	0.079	60
180	137	1.57	310	0.096	0.072	60
180	139	1.58	312	0.097	0.065	70
315	23	0.63	125	0.016	0.923	30
315	25	0.69	135	0.018	0.910	30
315	27	0.74	146	0.021	0.896	30
315	29	0.79	156	0.024	0.882	30
315	31	0.84	166	0.028	0.866	30
315	33	0.89	177	0.031	0.850	30
315	35	0.95	187	0.035	0.834	30
315	37	1.00	197	0.039	0.817	30

E [MeV]	θ [°]	Q [fm^{-1}]	Q [MeV/c]	Q^2 [(GeV/c)^2]	ϵ	time [min]
315	39	1.05	206	0.043	0.799	30
315	41	1.10	216	0.047	0.781	30
315	43	1.14	226	0.051	0.763	30
315	45	1.19	235	0.055	0.744	30
315	47	1.24	245	0.060	0.725	30
315	49	1.29	254	0.065	0.706	30
315	51	1.33	263	0.069	0.686	30
315	53	1.38	272	0.074	0.667	30
315	55	1.42	281	0.079	0.647	30
315	57	1.47	290	0.084	0.628	30
315	59	1.51	298	0.089	0.608	30
315	61	1.55	307	0.094	0.589	30
315	63	1.60	315	0.099	0.569	30
315	65	1.64	323	0.104	0.550	30
315	67	1.68	331	0.110	0.531	30
315	69	1.72	339	0.115	0.512	30
315	71	1.76	347	0.120	0.494	30
315	73	1.80	354	0.126	0.475	30
315	75	1.83	362	0.131	0.457	30
315	77	1.87	369	0.136	0.439	30
315	79	1.91	376	0.141	0.421	30
315	81	1.94	383	0.147	0.404	30
315	83	1.97	390	0.152	0.387	30
315	85	2.01	396	0.157	0.371	40
315	87	2.04	403	0.162	0.354	50
315	89	2.07	409	0.167	0.338	60
450	23	0.90	178	0.032	0.923	30
450	25	0.98	193	0.037	0.910	30
450	27	1.05	207	0.043	0.896	30
450	29	1.13	222	0.049	0.882	30
450	31	1.20	236	0.056	0.866	30
450	33	1.27	251	0.063	0.850	30
450	35	1.34	265	0.070	0.833	30
450	37	1.41	279	0.078	0.816	30
450	39	1.48	293	0.086	0.799	30
450	41	1.55	306	0.094	0.780	30

E [MeV]	θ [°]	Q [fm^{-1}]	Q [MeV/c]	Q^2 [(GeV/c)^2]	ϵ	time [min]
450	43	1.62	320	0.102	0.762	30
450	45	1.69	333	0.111	0.743	30
450	47	1.75	346	0.120	0.724	30
450	49	1.82	359	0.129	0.705	30
450	51	1.88	371	0.138	0.685	30
450	53	1.94	384	0.147	0.666	30
450	55	2.01	396	0.157	0.646	30
450	57	2.07	408	0.166	0.626	30
450	59	2.13	419	0.176	0.607	30
450	61	2.18	431	0.186	0.587	30
450	63	2.24	442	0.196	0.568	40
450	65	2.30	453	0.205	0.548	60
450	67	2.35	464	0.215	0.529	70

References

[1] R. Hofstadter, H. R. Fechter and J. A. McIntyre, Phys. Rev. **92** (1953) 978. E. E. Chambers and R. Hofstadter, Phys. Rev. **103** (1956) 1454.

[2] J. C. Bernauer *et al.* [A1 Collaboration], Phys. Rev. Lett. **105** (2010) 242001 [arXiv:1007.5076 [nucl-ex]].

[3] P. J. Mohr, B. N. Taylor and D. B. Newell, Rev. Mod. Phys. **80** (2008) 633 [arXiv:0801.0028 [physics.atom-ph]].

[4] I. Sick and D. Trautmann, Nucl. Phys. **A537** (1998) 449.

I. Sick, Prog. Part. Nucl. Phys. **47** (2001) 245 [nucl-ex/0208009].

[5] R. Pohl, A. Antognini, F. Nez, F. D. Amaro, F. Biraben, J. M. R. Cardoso, D. S. Covita and A. Dax *et al.*, Nature **466** (2010) 213.

[6] R. Pohl, A. Antognini, *et al.*, the CREMA Collaboration, private communication.

[7] R. W. Berard, F. R. Buskirk, E. B. Dally, J. N. Dyer, X. K. Maruyama, R. L. Topping and T. J. Traverso, Phys. Lett. B **47** (1973) 355.

[8] G. G. Simon, C. Schmitt and V. H. Walther, Nucl. Phys. A **364** (1981) 285.

[9] S. Platchkov, A. Amroun, S. Auffret, J. M. Cavedon, P. Dreux, J. Duclos, B. Frois and D. Goutte *et al.*, Nucl. Phys. A **510** (1990) 740.

[10] D. Abbott *et al.* [JLAB t20 Collaboration], Eur. Phys. J. A **7** (2000) 421 [nucl-ex/0002003].

[11] K. I. Blomqvist, W. U. Boeglin, R. Bohm, M. Distler, R. Edelhoff, J. Friedrich, R. Geiges and P. Jennewein *et al.*, Nucl. Instrum. Meth. A **403** (1998) 263.

[12] Ingo Ewald: *Entwicklung und Erprobung einer langen, dünnen Flüssig-Wasserstoff-Targetzelle*, Institut für Kernphysik der Universität Mainz, Diploma thesis, 1996

[13] Jan C. Bernauer: *Vorbereitung zur hochpräzisen Messung des elektrischen und magnetischen Formfaktors von Protonen*, Institut für Kernphysik der Universität Mainz, Diploma thesis, 2004.
Jan C. Bernauer: Measurement of the elastic electron-proton cross section and separation of the electric and magnetic form factor in the Q^2 range from 0.004 to 1 $(\mathrm{GeV/c})^2$, Institut für Kernphysik der Universität Mainz, Doctoral thesis, 2010.